Interferometric nulling of four channels with integrated optics

RONNY ERRMANN[1,2], STEFANO MINARDI[2,*], LUCAS LABADIE[3], BALAJI MUTHUSUBRAMANIAN[3], FELIX DREISOW[2], STEFAN NOLTE[2], AND THOMAS PERTSCH[2]

[1]*Astrophysical Institute and University Observatory, Friedrich-Schiller-Universität Jena, Schillergäßchen 2-3, 07745 Jena, Germany*
[2]*Institute of Applied Physics, Abbe Center of Photonics, Friedrich-Schiller-Universität Jena, Max-Wien-Platz 1, 07743 Jena, Germany;*
[3]*Physikalisches Institut, Universität zu Köln, Zülpicherstr. 77, 50937 Köln, Germany*
[*]*Corresponding author: stefano@stefanominardi.eu*

Compiled May 19, 2015

Nulling interferometry has been identified as a competitive technique for the detection of extrasolar planets. In its basic form, the technique consists in combining out-of-phase a single pair of telescopes to null effectively the light of a bright star an reveal the dim glow of the companion. However, in order to mitigate the effect of the stellar leaks through the interferometer, a broad angular central null is required. The hierarchical combination of several pairs of telescopes can accomplish this task. We have manufactured and tested with monochromatic light an integrated optics component which combines a linear array of 4 telescopes in the nulling mode envisaged by Angel&Wolf.[1] By simulating in the laboratory the the motion of a star in the sky, we could measure the expected angular transmission of the 4 telescope nuller. Moreover, the tests have demonstrated a broad nulling scaling as the fourth power of the baseline delay.

OCIS codes: *(130.3120) Integrated optics devices; (120.3180) Interferometry; (350.1260) Astronomical optics.*

http://dx.doi.org/10.1364/ao.XX.XXXXXX

1. INTRODUCTION

Simultaneous high-contrast and high-resolution observation of astronomical objects is a challenging front-end of modern observational astronomy, and a key for the direct detection and characterization of extrasolar planets. Nulling interferometry has been since long identified as a unique and competitive technique to perform mid-infrared spatially resolved spectroscopy of Earths and Super-Earths orbiting nearby main- sequence stars [2, 3]. The original Bracewell setup [4] consisted in phase-shifting one of the beam of a 2-telescope Michelson-type interferometer by 180 degrees in order to cancel out by destructive interference the signal of the on-axis bright star and simultaneously reveal the dim glow of a companion located at an angular distance of $\lambda/(2B)$ from the central star, where λ is the observing wavelength and B the interferometer baseline. A limitation of the Bracewell approach is the increased stellar leaks with increasingly large baselines, making planets at close angular distance from the parent star difficult to detect. A more sophisticated approach to nulling interferometry consists in implementing multi-baseline nulling configurations to broaden the central null, which allows to further reduce the stellar leaks when longer baselines – *i.e.* higher angular resolution – are used. Multi-aperture nulling also allows to modulate out the centro-symmetric exo-zodiacal signal that would otherwise hamper the faint planet signal. The inherent complexity of the beam combination stage in a spaceborne multi-aperture interferometer has always been a pitfall for nulling, together with the question of formation-flying. While it has been often suggested that an integrated optics (IO) and photonics-based approach would highly simplify the optical design of such an instrument [5], this was experimentally tested only at the level of a simple two-aperture interferometer based on the Bracewell configuration [6, 7], which mitigates the advantage of the multi-aperture interferometry approach. Four-beam bulk-optics, interferometric nulling concepts have been successfully studied at JPL with the Planet Detection Testbed [8], however the potential of integrated optics beam combiners to implement a four-telescope – or more – configuration has never been investigated in the past.

Here we concentrate on exploring a four-beam combination nulling scheme based on cascaded system of 2×2 directional couplers. The directional couplers have two inherent π phase-shifted outputs (i.e. a bright and a dark output), which does not require the insertion of an additional phase shifter stage. Combining together the nulled outputs of the directional couplers is the condition for producing a broader dark fringe, as compared

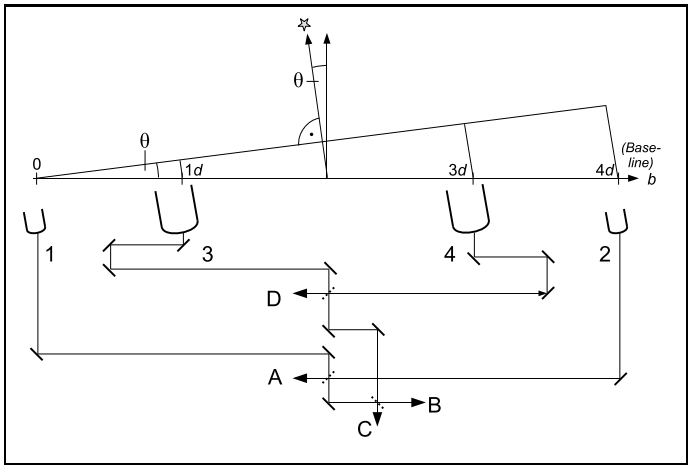

Fig. 1. The configuration of the four-telescope nuller after Angel & Woolf[1]. The inner telescopes (3 & 4) are spaced by a distance $2d$, while the outer ones (1 & 2) with half diameter are spaced by $4d$. Two beam splitters are used to combine at first the light of the inner and outer telescopes and, with a third splitter, their nulled outputs.

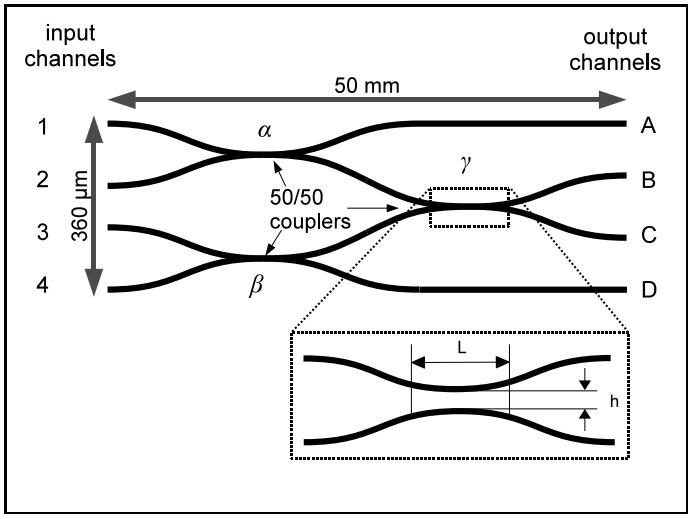

Fig. 2. Sketch of the photonic chip, featuring 3 directional couplers (α, β, γ) with 50/50 coupling ratio each. The number of the input channels correspond to the number of the telescope in Fig.1. In the inset we show the geometry of the couplers.

to the ones produced by the Bracewell setup. In this paper, the objective is twofold: first we wish to demonstrate the possible implementation of a four-telescope nulling scheme based on the usage of integrated optics. Second, we wish to assess experimentally the possibility to achieve a sixth power dependence of the transmission of the interferometer for small angular detunings from central null. In this work, the accent is set on showing the proof-of-concept of an integrated optics four-telescope nuller rather than on achieving a deep level of nulling of several 10^{-6}. We therefore report, for the first time to our knowledge, the characterization of an integrated optical component designed to combine in nulling mode four telescopes. Our investigation has been conducted at visible wavelengths ($\lambda = 633$ nm), but the emergence of new photonics solutions operational in the 10 μm spectral range [9] justifies the importance of our approach.

2. THE 4-TELESCOPE NULLER

Efficient interferometric rejection of light from the stellar disk requires at least two telescopes separated by a short baseline [4]. However, the simple Bracewell setup prevents the detection of sources at close angular separation from the star, as the small baseline does not allow full constructive interference of the light from the planet. One solution is to use two pairs of telescopes, one pair with small distance to suppress efficiently the stellar light and the other, with bigger distance, to obtain high resolution fringes[1]. The outputs of both nulled interferometers are then combined to obtain an angularly broad null.

Angel&Wolf [1] first proposed to use multiple telescopes to flatten the angular transmission of the interferometer in nulling mode. In their scheme, a linear array of 4 telescopes is foreseen (Fig. 1), with the inner ones separated by a distance of $2d$ and the outer ones placed at a distance of d beyond the inner ones (*i.e.* they are separated by a distance $4d$). The inner telescopes have twice the diameter of the outer ones, hence collect four times the flux from the target. The flux collected by the telescopes is interferometrically combined by a cascade of three 50/50 beam splitters distributed over two levels. At the first level, light from the inner and outer telescopes is mixed pairwise and phased in order to obtain a null at one output of each beam splitter. At the second level, both nulled outputs are combined by the third beam splitter. The main advantage of this scheme is that a broad angular transmission minimum can be achieved, allowing the effective nulling of light from partially resolved stars and mitigating the challenge of high accuracy fringe tracking.

A. Laboratory implementation

A planar integrated optics implementation of the Angel & Woolf beam combiner is straightforward. Free space optical paths are substituted by waveguides, while the beam splitters are replaced by 50/50 directional couplers arranged the a two-level cascade shown in Fig. 2. The light from the telescopes of Fig. 1 is coupled into the corresponding labeled waveguides of Fig. 2. In this way, the first two directional couplers combine the light of the external and internal telescopes, respectively. Two outputs from the first level of combination (one for each coupler) are then mixed by a third directional coupler. The dimensions of the manufactured integrated optical circuit were 0.36×50 mm.

To simulate the four telescope array, we used a modified Mach-Zehnder interferometer (see Fig. 3), which is used to prepare 4 beams out of a collimated and astigmatically shaped He-Ne laser beam ($\lambda = 633$ nm). The astigmatic beam shaping increases the coupling efficiency into the fabricated waveguides, as their supported modes are elliptical ($8.5 \times 5.5\,\mu$m, height $\times$ width, FWHM) [10]. The four, nearly-collinear beams are focused with a microscope (NA$=$ 0.25) at the input of the photonic chip. Each beam is coupled to the corresponding waveguide by acting on the horizontal tilt of the beam before the microscope objective. Brightness adjustment to precisely set the flux of two beams to a quarter of the other two was accomplished by the combination of a linear polarizer (inserted just before the microscope objective) and rotatable $\lambda/2$ plates inserted in the path of three beams.

To detect the output channels of the photonic chip, we used a microscope equipped with a 10-bit CCD camera. The magni-

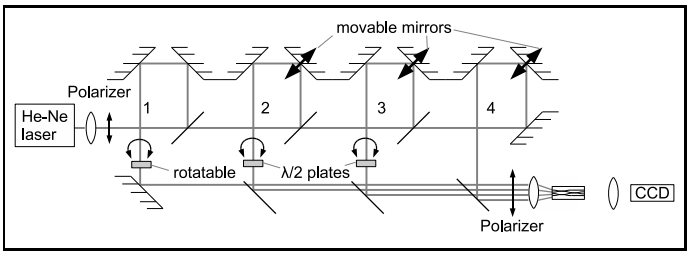

Fig. 3. Layout of the modified Mach-Zehnder interferometer used to simulate a linear array of 4 telescopes.

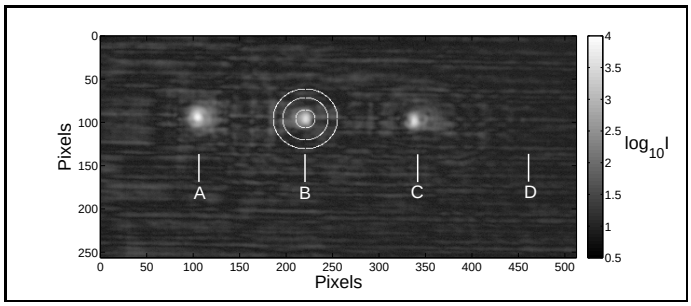

Fig. 4. Intensity distribution at the output face of the chip in logarithmic scale. The IO circuit was excited at channel 1. Due to the setup of the IO-device (Fig. 2) the output D remains dark. The 10 pixel (10.2 μm) aperture as well as the ring for the background measurements between 25 and 35 pixel (25.4 − 35.6 μm) are displayed around output B. The aperture covers about 90% of the flux, the fluxes outside the aperture are lower than 0.2% of the brightest pixel.

fication of the imaging system was such that the plate scale on the CCD was nearly exactly 1 μm/pixel.

The key to simulate the angular response of the linear 4-telescope array is to consider that a small angular shift θ of the astronomical target (*e.g.* a star) corresponds to a phase shift $\Delta\varphi_i$ of the starlight wavefront collected by telescope i which is proportional to the baseline length b_i between telescope i and the reference telescope 1 (see Fig. 1):

$$\Delta\varphi_i \simeq \frac{2\pi b_i \theta}{\lambda}. \quad \textbf{(1)}$$

In our case, b_i takes the values of 0, 4d, d, and 3d for telescope number ranging from 1 to 4. The angular scan can thus be converted to a phase scan of the input channels 2-4 with respect to the reference channel 1. We implemented the phase scan by inserting a movable mirror in three of the 4 arms of our modified Mach-Zehnder interferometer. The moveable mirrors were fabricated by attaching a mirror to the membrane of a loudspeaker. Sawtooth voltages with same periodicity and phase but different amplitude were applied to the loudspeakers to reproduce the transit of a source across the Zenith (Fig. 1). The linear ramps of the voltages correspond to maximum relative phase delays of 8π, 2π, and 6π for channels 2 to 4. This is the minimal phase delay configuration allowing to test one period of the angular response of the 4-telescope interferometer.

3. FABRICATION AND CHARACTERIZATION OF THE PHOTONIC CHIP

2×2 directional couplers based on the evanescent coupling between adjacent waveguides were implemented in the photonic circuit of the 4-telescopes nuller. In this kind of couplers, the splitting ratio depends on the length L of the region where the waveguides are adjacent and their separation h (see inset in Fig. 2). The photonic circuits were manufactured by means of ultrafast laser inscription, which allows fast prototyping of low loss ($\sim$ 0.3 dB/cm) single mode optical waveguides in silica substrates [11]. To achieve coupling ratios as close as possible to 50/50, we produced several photonic circuits made by identical couplers where L was kept fixed to 10 mm and the separation h between the adjacent waveguides was varied between 17 and 19 μm by steps of 0.5 μm. After measuring the splitting ratios of the couplers for each of the fabricated circuits, we found that the separation $h = 18\,\mu$m corresponded to the best approximation to the ideal 50/50 ratio (see Table 1).

The measurements of the splitting ratios were performed by coupling light of one of the beams from the Mach-Zehnder interferometer consecutively into each of the four input waveguides of the photonic circuit and measuring the transmitted power at the output waveguides by means of aperture photometry. In aperture photometry, the flux density inside an circular aperture centered at an output waveguide is integrated in space. The background flux, measured similarly over a ring around the center of the waveguide, is then subtracted. We used a 10.2 μm radius for the aperture and a ring with radius between 25.4 and 35.6 μm for the background measurements. With this choice of the inner ring, 90% of the flux carried by the mode of the waveguide could be collected. Fig. 4 displays the CCD output image of the input injection to channel 1 in logarithmic scale. Around output B the aperture and ring for background measurement are plot.

Assuming the same losses in all waveguides of the integrated optical circuit, we used the measured output fluxes for single input waveguide excitation to infer the splitting ratios.

The splitting ratios for our best sample are listed in Table 1. In the splitting ratios, the first number is defined as the percentage residual flux in the injection waveguide of the coupler divided by the total coupled power. The second number is the complement to 100% of the first number and represents the flux evanescently coupled to the non-excited waveguide, again normalized to the total coupled power. Because each coupler could be excited at least with two input configurations, we could estimate the error of our measurement as the standard deviation of multiple measurements.

As reported in the Table, nearly 50/50 splitting ratio was achieved for all 3 couplers. The small deviations from the ideal coupling ratio could be caused by interference of the output signal with stray light, fabrication defects (small variation of the inter-waveguide distance d) as well as by radiation losses occurring in the curved paths of the waveguides, which were not accounted for.

4. NULLING EXPERIMENT

As mentioned, the goal of the nulling experiment was twofold. From one side, we needed to proof that the ultrafast laser inscription fabrication process could deliver IO components of adequate quality to manufacture a 4-beams nulling beam combiner with transmission properties similar to what theoretically expected for bulk optics beam combiners. On the other side, we were interested in characterizing the shape of the flat null

Table 1. Splitting ratios at a wavelength of $\lambda = 633$ nm for the 3 couplers of Fig. 2 and their estimated uncertainty. See text for the definition of the splitting ratios.

coupler	splitting ratio	standard deviation
α	49.2/50.8	$\pm$0.4%
β	49.7/50.3	$\pm$3.4%
γ	48.2/51.8	$\pm$2.2%

and, to a lesser extent, its depth. To this end, we coupled the 4 beams of the Mach-Zehnder interferometer to the input waveguides of the selected IO circuit. We carefully adjusted the $\lambda/2$ plates so that the power coupled to waveguides 1 and 2 was exactly four times the power coupled to waveguides 3 and 4. The adjustment was monitored in real time by a LabView computer program performing the aperture photometry of the output waveguides A, B, C and D.

The optical path differences between the input beams were scanned with the method described in section 2.A. We set the fundamental phase scan rate to ~ 2.5 rad/s, which corresponds to a period of 2.5 s of the full fringe cycle. The absolute phase shift between the channels was fixed before turning on the phase scan by trimming the bias values of the electric driver of the phase modulators in such a way that of the outputs B and C were nulled.

Fig. 5 shows two periods of the 4-telescope fringes observed at the output port B and C of the chip. The data sampling frequency was set to 30 Hz and smoothing over 3 data points were applied to reject noise. The background flux has been estimated as indicated in Section 3 and subtracted to the raw interferogram. The fringes consist of an alternating sequence of narrow and broad minima, as expected in the 4-telescope nulling scheme. Overlaid as a dashed line is the normalized theoretical transmitted intensity by the interferometer following $T = 4[\sin(\phi)^2] \cdot [\sin(\phi/2)^4]$, with alternating null dependency as $\sim \phi^2$ and $\sim \phi^6$. We can also observe the π phase shift between outputs B and C as expected for a directional coupler. This result shows the quality of the fabricated IO component is adequate to reproduce the expected shape of a linear 4-telescope nulling beam combiner.

The next step has been the characterization of the flat null and its depth. The lower plot of Fig. 5 shows the normalized rejection ratio measured with our combiner, which is found to be a fraction of 1:100 of the maximum flux. This result is discussed in Sect. 5. Afterwards, in order to measure the power law dependence on the phase of the interferometric signal at the broad-minima, we fitted the data of a few different minima with the function $y = a(\phi - b)^c + d$, where ϕ is the phase variable, b and d respectively the horizontal and vertical offsets estimated by hand, and a and c the free parameters of the fit. We used for that purpose the Python **curve_fit** routine from the **SCIPY** package. The fit was estimated over a ± 1 rad phase range around the fringe minimum, which is nonetheless larger than the angular size seen by the interferometer of a Sun at 5 pc (see caption Fig. 5).

Fig. 6 illustrates the result of such a fit for two good quality nulls for which we find a best fit a_1=1302$\pm$53 and a_2=1181$\pm$67 for the slope parameter, c_1=4.89$\pm$0.36 and c_2=4.21$\pm$0.45 for the

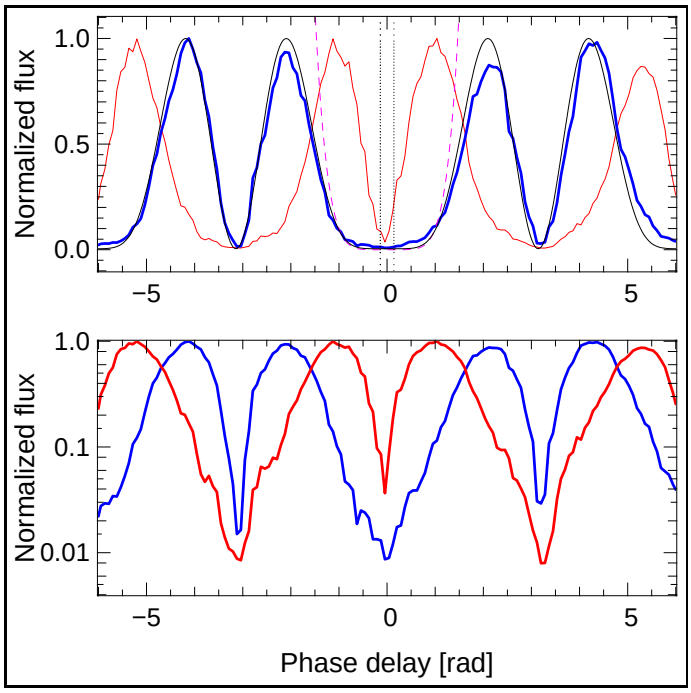

Fig. 5. Outputs B (red) and C (blue) of the photonic chip as a function of the phase delay in radians. The 2π period corresponds to $\sim$ 5 s in time. Smoothing over 3 data points ($\sim$ 0.1 s) has been applied. (Top) The normalized fringe flux is plotted in linear scale alongside with the theoretical fringe pattern dependency derived by Angel & Wolf (black continuous line) and the $0.1x^6$ function (magenta dashed line). The two vertical dotted lines show the extent of the stellar disc for a Sun at 5 pc observed with an outer baseline B=100m and at $\lambda = 10\mu$m. (Bottom): Visualization of the raw rejection ratio in logarithmic scale (see Text for details). The null is measured in the best case to a fraction of 1:100 of the maximum flux.

exponent parameter. To assess the "goodness of fit" between the experimental and fitted data, we compute the reduced χ^2_r between the two distributions with c varying linearly from 3.0 to 7.0. For each fixed value of c, a is then best fitted with the **curve_fit** routine. The lower plots of Fig. 6 show that a minimum χ^2_r is obtained for, respectively, c=4.8 and 4.6 in agreement with the values of c_1 and c_2. The reduced χ^2_r is found to be $\sim$1.03 showing good agreement with the experimental data.

5. DISCUSSION

The experiment shows that our integrated optics, 4-telescope beam combiner can generate a broad angular null, albeit not as wide and deep as theoretically expected. We obtain a best-null of $\sim 8\times10^{-3}$ and a $\sim\theta^{4.5}$ dependence of the broader dark fringe. It is well known that deep nulling is very sensitive to intensity, phase and polarisation mismatches between the beams to be combined. Our results can be discussed under these considerations, suggesting technical improvements in the testbed and the IO component that could ameliorate the null properties.

A possible cause for the limited measured values is the deviation of the actual splitting ratios of the directional couplers from the ideal value of 50:50 as shown in Table 1, which would result in intensity mismatches. However, we discarded this hypothesis after comparing the experimental results to the numer-

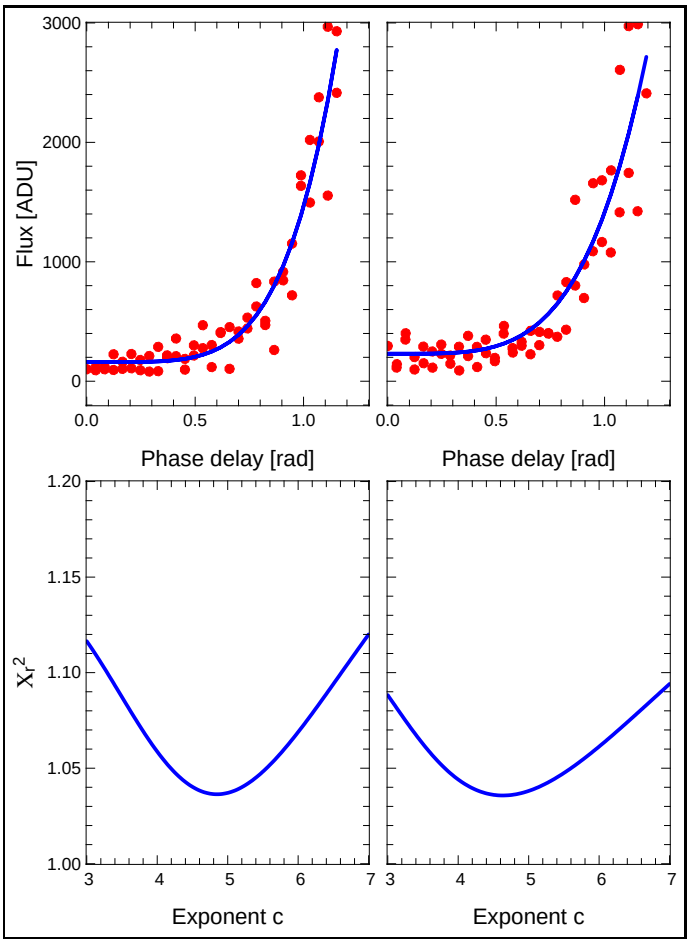

Fig. 6. Result of the fit of 2 broad minima of the interference time series with a power-law dependence $y = a(\phi - b)^c + d$. *Top:* The data are mirrored around the value $\phi_2 = b$. Best fit is found, respectively for fringe 1 (left) and 2 (right), for a=[1302±53,1181±67] and c=[4.89±0.36,4.21±0.45]. *Bottom:* χ_r^2 minimization to derive the exponent c of the upper fringe. A minimum χ_r^2 value of ∼1.03 shows good agreement with the experimental data for c=[4.8,4.6].

ical simulation of the actual IO circuit. This is illustrated in the plot of Fig. 7, where the data of the best fringe of Fig. 6 are plotted in bi-logarithmic scale, which transforms power-laws dependences into lines. Accounting for the measured splitting ratios, the graph shows that for phase detuning smaller than 0.15 rad the angular transmission of the photonics chip should reach a constant floor of 10^{-4} – which is significantly lower than the measured floor – while for larger phase-detuning the decay should theoretically follow the θ^6 power-law. The splitting-ratio deviations of our chip are in principle kept small enough to allow a deeper extinction.

Lower null exponents and extinction can probably be explained by a fluctuation of the phase bias between the four input light beams due to acoustic noise and thermo-mechanical stresses in our delay lines. We indeed employ an interferometer simulator setup with no control loop and feedback for the position of the phase actuators. This likely implies that the phase relationships between the interfering beams are not accurate and stable enough to achieve a deep null. Not surprisingly, previous deep null demonstrations have an accurate control of the phases implemented through a metrology system and a feedback loop.[8]. In our case, such phase variations distort asymmetrically the angular transmission function, and reduce the power-law and depth of the null fringe.

Despite using a single-mode photonics chip, mismatches can also occur between the respective TE and TM polarisation of the propagated wavefronts. While this need further dedicated investigation, such an issue is typically solved by placing an output polariser to separately treat the two polarisations.

Regarding the testbed, an additional limitation of our setup is the detection camera, which has a dynamic of only 10 bits. This means that the minimal detected flux is $\sim 10^{-3}$ times the saturation flux. In our measurements, the background of the images was very close to the minimal detectable flux (0.2-0.3% of the peak - see Fig. 4). The use of a 14 bit or 16 bit camera or high dynamics photodiodes connected to the output waveguides would definitely allow a better dynamic of the measurements.

The second category of improvements regards the photonic beam combiner itself. In our design, we cannot eliminate completely the stray light resulting from excitation of radiating modes at the input of the waveguides and along the waveguide bends. Because of interferometric amplification, this weak background could distort considerably stronger guided signals and prevent the measurement of a deep null. Injection points inclined respect to the output plane [6] or spatial offset from the output waveguides [12] would reduce considerably the radiation background and therefore deepening the achievable null.

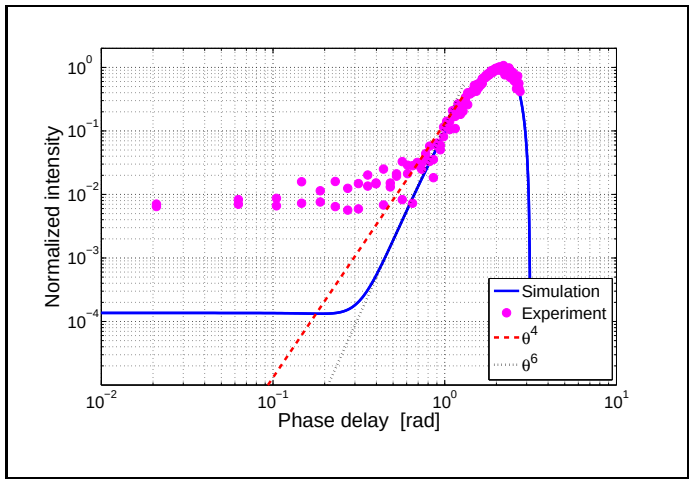

Fig. 7. Dependence of the interferometric signal as a function of the phase detuning from the center of the broad minimum in bi-logarithmic scale. Experimental data (dots) are taken from fringe no. 1 in Fig. 6. The continuous line represents the simulated transmission from a numerical model of our IO component, featuring the measured splitting ratios of the directional couplers. The dashed line is the θ^4 dependence while the dotted line represents the θ^6 trend.

6. CONCLUSIONS

Our investigation on the application of integrated optics technology to multi-telescope nulling resulted in clearly identifying advantages and pitfalls of the IO approach to multi-telescope nulling interferometry. Among the advantages, we certainly mention the compact size and the virtual absence of degrees of

freedom of the IO approach which are essential features for future space- borne interferometers. Our choice of the direct laser writing manufacturing technique is also motivated by the fact that it can enable IO in the mid-infared [14], the most interesting band for exoplanet detection. The best achievable attenuation has been just below 1:100 with a $\theta^{4.5}$ dependence of the null in the Angel&Wolf linear scheme. Analysis of the data evidenced the limitations of our experimental arrangement, in particular regarding the absolute phase stability of the multi-path Mach-Zehnder interferometer, but also in potential issues related to the design of the IO component (radiating modes background). In particular, we noticed how the stray light originating from the mode shape mismatch at the injection of the component or from the radiation losses of bended waveguides could contribute to raise the background to the level of several 10^{-3} of the maximum waveguide output. While our component featured narrow-band directional couplers, we mention that the manufacturing of achromatic couplers operating on a broad-band is possible [13, 15] and could be investigated in the future.

REFERENCES

1. Angel, J. R. P. and Woolf, N. J., "An Imaging Nulling Interferometer to Study Extrasolar Planets," *The Astrophysical Journal* **475**, 373 (1997).
2. Léger, A., Defrère, D., Malbet, F., Labadie, L. and Absil, O., "Impact of η-earth on the capabilities of affordable space missions to detect biosignatures on extrasolar planets," *arXiv:1504.08232*
3. Labadie, L., Léger, A., Malbet, F., Danchi, W. C., and Lopez, B., "A possible future for space-based interferometry," in [*Improving the Performances of Current Optical Interferometers & Future Designs*], Arnold, L., Le Coroller, H., and Surdej, J., eds., 47–56 (2014).
4. Bracewell, R. N., "Detecting nonsolar planets by spinning infrared interferometer," *Nature* **274**, 780 (1978).
5. Labadie, L., Kern, P., Labeye, P., Lecoarer, E., Vigreux-Bercovici, C., Pradel, A., Broquin, J.-E., and Kirschner, V., "Technology challenges for space interferometry: The option of mid-infrared integrated optics," *Advances in Space Research* **41**, 1975–1982 (2008).
6. Weber, V., Barillot, M., Haguenauer, P., Kern, P. Y., Schanen-Duport, I., Labeye, P. R., Pujol, L., and Sodnik, Z., "Nulling interferometer based on an integrated optics combiner," in [*New Frontiers in Stellar Interferometry*], Traub, W. A., ed., *Society of Photo-Optical Instrumentation Engineers (SPIE) Conference Series* **5491**, 842 (2004).
7. Buisset, C. and Rejeaunier, X. and Rabbia, Y. and Barillot, M., "Stable deep nulling in polychromatic unpolarized light with multiaxial beam combination", *Applied Optics* **46**, 7817–7822 (2007).
8. Martin, S., Booth, A., Liewer, K., Raouf, N., Loya, F., and Tang, H., "High performance testbed for four-beam infrared interferometric nulling and exoplanet detection," *Applied Optics* **51**, 3907–3921 (2012).
9. Labadie, L. and Wallner, O., "Mid-infrared guided optics: a perspective for astronomical instruments," *Optics Express* **17**, 1947–1962 (2009).
10. Minardi, S., Dreisow, F., Gräfe, M., Nolte, S., and Pertsch, T., "Three-dimensional photonic component for multichannel coherence measurements," *Optics Letters* **37**, 3030–3032 (2012).
11. Pertsch, T., Peschel, U., Lederer, F., Burghoff, J., Will, M., Nolte, S., and Tünnermann, A., "Discrete diffraction in two-dimensional arrays of coupled waveguides in silica," *Optics Letters* **29**, 468–470 (2004).
12. Jovanovic, N., Tuthill, P. G., Norris, B., Gross, S., Stewart, P., Charles, N., Lacour, S., Ams, M., Lawrence, J. S., Lehmann, A., Niel, C., Robertson, J. G., Marshall, G. D., Ireland, M., Fuerbach, A., and Withford, M. J. "Starlight demonstration of the Dragonfly instrument: an integrated photonic pupil-remapping interferometer for high-contrast imaging," *MNRAS* **427**, 806 (2012).
13. Benisty, M., Berger, J.-P., Jocou, L., Labeye, P., Malbet, F., Perraut, K., and Kern, P. "An integrated optics beam combiner for the second generation VLTI instruments," *A&A* **498**, 601 (2009).
14. Gross, S., Jovanovic, N., Sharp, A., Ireland, M., Lawrence, J., and Withford, M. J. "Low loss mid-infrared ZBLAN waveguides for future astronomical applications,"*Opt. Exp.* **23**, 7946–7956 (2015).
15. Hsiao, H.-K., Winick, K. A., and Monnier, J. D. "Midinfrared broadband achromatic astronomical beam combiner for nulling interferometry," *Applied Optics* **49**, 6675 (2010).